Non-isothermal modification of purely elastic flow instabilities in torsional flows of polymeric fluids

Jonathan P. Rothstein and Gareth H. McKinley
Department of Mechanical Engineering, Massachusetts Institute of Technology, Cambridge, Massachusetts 02139

(Received 29 February 2000; accepted 4 November 2000)

Previous experimental measurements and linear stability analyses of curvilinear shearing flows of viscoelastic fluids have shown that the combination of streamwise curvature and elastic normal stresses can lead to flow destabilization. Torsional shear flows of highly elastic fluids with closed streamlines can also accumulate heat from viscous dissipation resulting in nonuniformity in the temperature profile within the flow and nonlinearity in the viscometric properties of the fluid. Recently, it has been shown by Al-Mubaiyedh *et al.* [Phys. Fluids **11**, 3217 (1999)] that the inclusion of energetics in the linear stability analysis of viscoelastic Taylor–Couette flow can change the dominant mode of the purely elastic instability from a nonaxisymmetric and time-dependent secondary flow to an axisymmetric stationary Taylor-type toroidal vortex that more closely agrees with the stability characteristics observed experimentally. In this work, we present a detailed experimental study of the effect of viscous heating on the torsional steady shearing of elastic fluids between a rotating cone and plate and between two rotating coaxial parallel plates. Elastic effects in the flow are characterized by the Deborah number, De, while the magnitude of the viscous heating is characterized by the Nahme–Griffith number, Na. We show that the relative importance of these two competing effects can be quantified by a new dimensionless thermoelastic parameter, $\Theta = \mathrm{Na}^{1/2}/\mathrm{De}$, which is a material property of a given viscoelastic fluid independent of the rate of deformation. By utilizing this thermoelastic number, experimental observations of viscoelastic flow stability in three different fluids and two different geometries over a range of temperatures can be rationalized and the critical conditions unified into a single flow stability diagram. The thermoelastic number is a function of the molecular weight of the polymer, the flow geometry, and the temperature of the test fluid. The experiments presented here were performed using test fluids consisting of three different high molecular weight monodisperse polystyrene solutions in various flow geometries and over a large range of temperatures. By systematically varying the temperature of the test fluid or the configuration of the test geometry, the thermoelastic number can be adjusted appreciably. When the characteristic time scale for viscous heating is much longer than the relaxation time of the test fluid ($\Theta \ll 1$) the critical conditions for the onset of the elastic instability are in good agreement with the predictions of isothermal linear stability analyses. As the thermoelastic number approaches a critical value, the strong temperature gradients induced by viscous heating reduce the elasticity of the test fluid and delay the onset of the instability. At even larger values of the thermoelastic parameter, viscous heating stabilizes the flow completely. [DOI: 10.1063/1.1338540]

I. INTRODUCTION

The torsional motion of a fluid between a rotating cone and plate and between two rotating coaxial parallel plates is used extensively in rheometry to measure the material properties that characterize non-Newtonian fluids. For highly elastic fluids, the combination of streamline curvature and large normal stresses in a torsional shear flow results in a streamwise tension that can destabilize the flow.[1,2] Beyond a critical rotation rate, experimental observations and linear stability analyses show that the steady, two-dimensional, torsional shearing motion becomes unstable to a three-dimensional, time-dependent flow with a spiral plan form.[3–6] The occurrence of instabilities in the processing of polymer melts and solutions has been understood for many years and has been well documented in reviews by Petrie and Denn[7] and Larson[8] while a detailed review of purely elastic flow instabilities in viscometric flows can be found in Shaqfeh.[9] In the present study, we will focus on the latter class of viscometric motion with closed streamlines in which inertial effects are vanishingly small and the purely elastic instability is strictly a result of the interaction between the viscoelasticity of the fluid and the curvature of the flow streamlines.

In any shear flow with closed streamlines, the test fluid can be exposed to high shear rates over an extended period of time. As a result of the poor thermal conductivity of typical polymeric materials, the accumulating heat from viscous dissipation can have a significant effect on the temperature profile and, hence, on the measured viscometric properties of the fluid. For a fluid undergoing a steady shearing deforma-

tion, the Nahme number quantifies the relative importance of viscous heating[10] and is given by

$$\mathrm{Na}=\frac{\eta_0\beta H^2\dot{\gamma}^2}{kT}, \tag{1}$$

where η_0 is the viscosity in the limit of zero shear rate, $H\dot{\gamma}=U$ is the characteristic velocity, k is the thermal conductivity, T is the absolute temperature, and β is the thermal sensitivity of the fluid viscosity, defined as

$$\beta=\frac{T}{\eta_0}\left(\left|\frac{d\eta}{dT}\right|\right). \tag{2}$$

Recognizing the onset of viscous heating is important in the study of polymer solutions and melts because the thermal sensitivity of the fluid tends to increase monotonically as the molecular weight and the viscosity of the fluid are increased.[11] Polymer melts are typically very viscous and, in highly elastic dilute polymer solutions, the solvent is often chosen to have a very large viscosity (denoted η_s) in order to increase the relaxation time of the polymer and reduce inertial effects.[12] Therefore, it is to be expected that viscous heating in polymeric fluids may significantly affect the stability of viscoelastic flows. In fact, some of these effects have already been observed. Nonpermanent reductions in the measured first normal stress difference after long periods of continuous shearing between a rotating cone and plate and parallel plate under unstable conditions were reported by both MacDonald and Muller[13] and Magda and Larson.[14] This long time stabilization of the flow is indicative of the accumulation of energy as a direct result of viscous dissipation, despite careful control of the thermal boundary conditions. Nonisothermal effects on the stability conditions of more complex viscoelastic flows have also been investigated[15] and the possibility of using thermal modulation for optimal control of viscoelastic flow has recently been considered.[16]

A number of theoretical studies have investigated the effect of viscous heating on the stability of shear flows. In the linear stability analyses of Newtonian planar Couette flow, viscous stratification induced by temperature gradients resulting from viscous heating was found to destabilize the flow at finite values of the Reynolds number.[17,18] However, at zero Reynolds number, the Newtonian plane shear flow was shown to be stable.[17] The addition of viscoelasticity does not destabilize the inertialess flow because of the poor coupling between the (stable) energy modes and the (stable) eigenmodes of the viscoelastic isothermal shear flow.[19] Isothermal viscoelastic Taylor–Couette flow, however, is unstable[1] even at zero Reynolds number because of the addition of streamline curvature. Detailed experimental investigations using highly viscous polymer solutions have reported the appearance of steady axisymmetric toroidal vortices following the loss of flow stability.[20] These observations directly contradict the nonaxisymmetric and time-dependent form of the secondary flow predicted by isothermal linear stability analysis.[1,9] Furthermore, the critical conditions for the onset of instability can differ by more than an order of magnitude from those observed experimentally.[13] Recent work by Al-Mubaiyedh *et al.* has demonstrated that

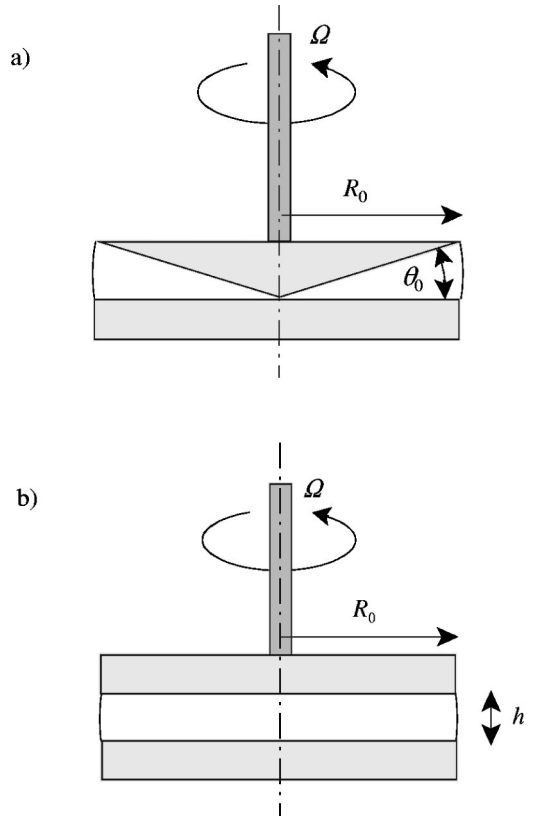

FIG. 1. Schematic diagram of the cone-and-plate and the parallel-plate geometries.

the form of the secondary flow observed experimentally can be predicted theoretically through inclusion of viscous heating terms in the linear stability analysis of the viscoelastic Taylor–Couette flow.[21] The resulting critical conditions are also much closer to the experimental observations. The effect of viscous heating on the stability boundaries of other torsional shear flows such as the flow between a rotating cone and plate and rotating coaxial parallel plates remain to be investigated. In the current work we address these issues.

Schematic diagrams of the cone-and-plate and parallel-plate geometries are shown in Fig. 1. In these devices, it is possible to alter the flow geometry by varying the radius, R_0, cone angle, θ_0, and gap height separating the test fixtures, h. The corresponding dimensionless parameter characterizing the flow geometry can be written as $\alpha^{\mathrm{pp}}=h/R_0$ for the parallel-plate configuration and as $\alpha^{\mathrm{cp}}=\theta_0$ for the cone-and-plate configuration. For small $\alpha\ll 1$, the base flow for each geometry is steady, two dimensional, and leads to measured values of torque, $\mathcal{T}$, and normal thrust, N, which in turn can be used to compute the deformation-rate-dependent viscosity, $\eta(\dot{\gamma})$, and the first normal stress coefficient, $\Psi_1(\dot{\gamma})$. As the differential angular velocity, Ω, between the upper and lower plates is increased, experiments have shown that the flow can become unstable. The critical flow conditions for the onset of this instability are typically reported in terms of a critical Deborah number,

$$\mathrm{De}_{\mathrm{crit}}=\lambda\Omega_{\mathrm{crit}}, \tag{3}$$

where λ is the characteristic relaxation time of the fluid and

TABLE I. Summary of analytical and numerical solutions to the isothermal cone-and-plate and parallel-plate linear stability problem. Note that $\mathrm{Wi}=\mathrm{De}/\alpha$ with $\alpha^{\mathrm{PP}}=h/R_0$ and $\alpha^{\mathrm{CP}}=\theta_0$.

Contributor	Description of work	Parallel-plate result	Cone-and-plate result
Phan-Thien (1983,1985) (Refs. 22 and 23)	• Oldroyd-B/UCM • Similarity solution	$\mathrm{De}_{\mathrm{crit}}=\dfrac{\pi}{\sqrt{(1-S)(1-2S)}}$	$\mathrm{De}_{\mathrm{crit}}=\pi\sqrt{\dfrac{2}{(1-S)(1-2S)}}$
Olagunju (1994,1995) (Refs. 4 and 5)	• Oldroyd-B/UCM • Short-wavelength solution	$\mathrm{De}_{\mathrm{crit}}=4.604\,f(S)\alpha^{1/2}$ $f(S)\sim(1-S)^{-1/2}$ for $S\to 1$	$\mathrm{De}_{\mathrm{crit}}=4.604\,f(S)\theta_0^{1/2}$ $f(S)\sim(1-S)^{-1/2}$ for $S\to 1$
Avagliano and Phan-Thien (1996) (Ref. 6)	• Oldroyd-B/UCM • Short-wavelength solution • Finite edge effects	$\mathrm{De}_{\mathrm{crit}}=K_1+\alpha K_2$ $0\leqslant K_1\leqslant 2$ $5\leqslant K_2\leqslant 10$	?

the characteristic residence time in the flow is equal to the inverse of the angular velocity, Ω. Alternatively, the critical conditions can be reported in terms of a critical Weissenberg number,

$$\mathrm{Wi}_{\mathrm{crit}}=\lambda\dot{\gamma}_{\mathrm{crit}}, \tag{4}$$

where $\dot{\gamma}_{\mathrm{crit}}$ is the critical deformation rate at which the flow becomes unstable. For both test geometries, $\dot{\gamma}=\Omega/\alpha$.

The stability of inertialess viscoelastic flows in cone-and-plate and parallel-plate geometries was first investigated analytically by Phan-Thien.[22,23] Using the von Karman similarity form for long-wavelength disturbances in an Oldroyd-B fluid, Phan-Thien was able to calculate critical Deborah numbers that were, for both cases, dependent only on the ratio of solvent to total viscosity, $S=\eta_s/\eta_0$, although the precise form of the dependence on S for the cone-and-plate geometry was later corrected by Olagunju.[24] Soon after, Magda and Larson[14] made the first quantitative experimental investigation of an elastic torsional flow instability. They observed the onset of a time-dependent increase in viscosity and first normal stress difference in tests run in both a cone-and-plate and a parallel-plate rheometer when the shear rate was increased above a critical value. Visual observations of the induced secondary flow by McKinley *et al.*[3] indicated that the flow transition was nonaxisymmetric, overstable in time, and subcritical in shear rate. These observations contradicted the theoretical analysis of Phan-Thien. This discrepancy was later resolved by Olagunju,[4,25] who showed that the most unstable disturbance is not the long-wavelength solution of Phan-Thien, but a short-wavelength mode of dimensionless wave number $O(\alpha)$. He went on to show that the critical Deborah number is not simply a function of S, but scales with $\alpha^{1/2}$. A weakly nonlinear stability analysis for the small cone-angle limit of the viscoelastic flow between a cone and plate was also performed by Olagunju.[26] The rheology of the test fluid was found to have a strong influence on the temporal form of the instability. For $S>0.02$, the flow transition was found to be a subcritical Hopf bifurcation in shear rate whereas in the small solvent viscosity limit, $S\leqslant 0.02$, the flow transition was found to be supercritical. The results of these analyses are in good agreement with the work of McKinley *et al.*[3,27] for the cone-and-plate geometry, but do not agree with the radially localized flow structure experimentally observed in the parallel-plate geometry because the analysis fails to include the influence of the free surface and the effect of shear thinning in the nonhomogeneous shearing flow.[28] The presence of a free surface at the edge of the parallel-plate geometry and the weak secondary flow that it induces were later included by Avagliano and Phan-Thien.[6] The analysis of Avagliano and Phan-Thien improved agreement between theory and experiment and showed that, when edge effects were considered, the critical Deborah number scaled linearly with the geometric parameter α^{PP}. Using an analytical model equation developed by Olagunju[25] that is valid in the limit of small gaps, Renardy and Renardy[29] were able to closely approximate the two-dimensional numerical results of Avagliano and Phan-Thien.[25,29] The effect of a free surface on the instability in cone-and-plate flow has yet to be investigated. A summary of the predicted forms of the critical conditions given by the theoretical and numerical isothermal linear stability analyses discussed above can be found in Table I.

The primary objective of the present experimental work will be to systematically characterize the effect of viscous heating and the resulting nonisothermal fluid temperature profiles on the onset conditions of purely elastic torsional flow instabilities. We have chosen the cone-and-plate and parallel-plate geometries because they allow for precise temperature control of the boundary, sensitive shear stress and first normal stress difference measurements and the flexibility to easily make significant changes in the dimensionless geometric parameter α.

The isothermal stability analyses presented in Table I suggest that the stability boundary can be represented on a two-dimensional plot of the Deborah number against the di-

TABLE II. Governing timescales of nonisothermal polymeric flows. Note that the characteristic length scale $H=h$ for parallel-plate geometries and $H=\theta_0 R$ for cone-and-plate geometries. The time scale for viscoelastic stress relaxation is indicated generically by λ; however, in reality, a polymeric fluid is characterized by a spectrum of time scales. A number of different average measures may therefore be used [see the text and Eqs. (11)–(16) for details].

Time scale	Dimensionless group (scaled with $t_{conv}=\dot{\gamma}^{-1}$)		Typical value
① $t_{thermal}=\frac{\rho C_p H^2}{k}$	Péclet number	$Pé=\frac{\rho C_p H^2\dot{\gamma}}{k}$	$\gg 1$
② $t_{diffusion}=\frac{\rho H^2}{\eta_0}$	Reynolds number	$Re=\frac{\rho H^2\dot{\gamma}}{\eta_0}$	$\ll 1$
③ $t_{polymer}=\lambda$	Weissenberg number	$Wi=\lambda\dot{\gamma}$	$\sim O(1)$
④ $t_{heat}=\sqrt{\frac{\eta_0 H^2\beta}{kT}}$	Nahme number	$Na=\frac{\eta_0 H^2\beta\dot{\gamma}^2}{kT}$	$\sim O(1)$
Natural ratios (material functions independent of kinematics)			
$\frac{①}{②}=\frac{t_{thermal}}{t_{diffusion}}$ = Prandtl number,		$Pr=\frac{\eta_0 C_p}{k}\gg 1$	
$\frac{③}{②}=\frac{t_{polymer}}{t_{diffusion}}$ = elasticity number,		$E=\frac{\lambda\eta_0}{\rho H^2}\gg 1$	
$\frac{④}{③}=\frac{t_{heat}}{t_{polymer}\alpha}$ = thermoelastic number,		$\Theta=\lambda R_0\sqrt{\frac{\eta_0\beta}{kT}}\sim O(1)$	

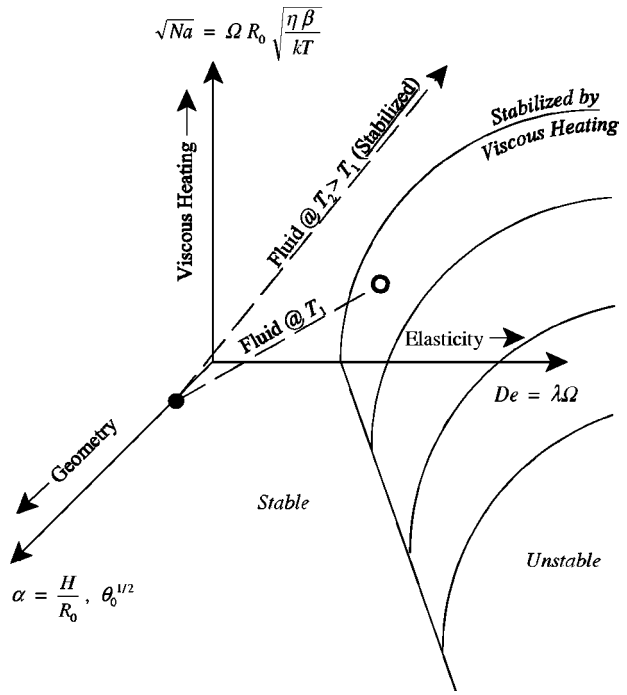

FIG. 2. Three-dimensional schematic stability diagram for a typical viscoelastic fluid.

mensionless geometric parameter. Such diagrams have been presented in previous publications.[2,3,9,27] Incorporating the effects of viscous heating leads to the study of the stability boundary off this plane. However, the proper dimensionless group to represent this third dimension is unclear. We explore possible three-dimensional representations of the stability diagram in Sec. II A and introduce a dimensionless thermoelastic parameter, Θ, characterizing viscous heating in a polymeric fluid. In Sec. II B, we briefly summarize the rheological characteristics of our test fluids and the actual values of the thermoelastic parameter for the dilute polystyrene solutions used in these experiments. In Sec. III, we first compare our experimental results for flow within a cone-and-plate and parallel-plate rheometer to isothermal linear stability analyses. The effect of viscous heating on the purely elastic flow instability is then demonstrated through experiments performed over a wide range of temperatures. Finally, in Sec. IV, we present our conclusions.

II. EXPERIMENT

A. Stability diagrams for nonisothermal viscoelastic flows

By nondimensionalizing the governing partial differential equations for momentum and energy, one can identify the time scales that characterize nonisothermal polymeric flows. These values are tabulated in Table II and include the time scales for thermal and viscous diffusion, the polymeric time scale for stress relaxation and the time scale for viscous heating. These time scales can be used to construct two types of dimensionless groups: (i) dynamical ratios that use the convective time as the characteristic scale and thus have values that depend on the shear rate; and (ii) intrinsic or material ratios that are independent of kinematics. This table suggests that a self-consistent set of dimensionless groups to use when considering the stability of viscoelastic flows are the Weissenberg number, which is a direct measure of the flow strength, in conjunction with the elasticity number, E, and thermoelastic number, Θ, which measure the intrinsic importance of the additional nonlinearities arising from inertia and/or viscous heating. Baumert and Muller[20] have reported extensively on the effect of varying the elasticity number on the stability boundaries of viscoelastic Taylor–Couette flow by preparing a set of fluids with differing solvent viscosities. Al-Mubaiyedh *et al.*[21] report their results in terms of a Péclet number (which will always be very large since $Pr\gg 1$ for all polymer melts and organic solutions) and a Brinkman number $Br=Na/\beta$ (which is always very small because $\beta\gg 1$). To our knowledge no one has yet experimentally investigated the importance of the thermoelastic number, which may be of $O(1)$ for elastic fluids undergoing a rapid shearing deformation. Systematic investigation of thermoelastic effects can be performed by preparing a set of viscoelastic fluids of different viscosities and/or relaxation times (by varying the molecular weight of the polymer or the viscosity of the solvent) and then conducting tests while varying the flow geometry and ambient temperature.

The combined effect of these variations on the thermoelastic number on the stability boundary for a typical elastic flow instability is shown graphically in Fig. 2. Here we select the Deborah number as a measure of the elastic effects and the Nahme number as a measure of the importance of viscous heating. When flow stability experiments are performed with a given fluid in a fixed flow geometry by slowly incrementing the deformation rate, $\dot{\gamma}$, the slope of the trajec-

tory in this three-dimensional space is given by the thermoelastic parameter

$$\Theta = \frac{\sqrt{\mathrm{Na}}}{\mathrm{De}} = \frac{R_0}{\lambda(T,M_w)} \sqrt{\frac{\eta_0(T,M_w)\beta(T)}{kT}}. \tag{5}$$

For very low values of the thermoelastic parameter, $\Theta \ll 1$ (corresponding ideally to fluids of low viscosity and high relaxation time) the stability boundary is expected to collapse to the form given in Table I. However, quite generally, we expect that when the two time scales are of comparable magnitude, viscous heating will affect the critical conditions for onset of the elastic instability.

For dilute polymer solutions, the Rouse–Zimm kinetic theory model predicts that the viscosity and the relaxation time are differing functions of the molecular weight.[30,31] For example, in the non-free-draining limit the Zimm model predicts that the polymeric contribution to the viscosity scales as $\eta_p \propto c\,\eta_s M_w^{1/2}/k_B T$ and $\lambda \propto M_w^{3/2}$, where c is the concentration, M_w is the molecular weight of the chain, and k_B is Boltzmann's constant. Thus, decreasing the molecular weight of the polymer will increase the relative importance of viscous heating. The geometry can also be adjusted to alter the extent of viscous heating at a given Deborah number, but the flexibility for geometric variation is quite limited for standard test fixtures because the analytical form of the base flow assumes $\alpha \ll 1$.

Another alternative, and the avenue down which we have proceeded, is to vary the experimental test temperature, T. As the temperature is increased, the thermoelastic number increases and the critical Deborah number for the onset of the purely elastic instability occurs at progressively larger Nahme numbers. At these large Nahme numbers, viscous heating will delay or even completely suppress the onset of the instability. This is indicated schematically in Fig. 2, but it may not be clear from a cursory inspection of Eq. (5). For amorphous viscoelastic materials, time–temperature superposition (TTS) can be used to characterize the temperature dependence of the material properties of the fluid.[10,32] The viscosity and relaxation time can be explicitly determined at a temperature, T, in terms of a time–temperature shift factor and the known material properties at a reference temperature, T_0, by

$$a_T(T,T_0) = \frac{\eta_0(T)}{\eta_0(T_0)} = \frac{\lambda(T)T}{\lambda(T_0)T_0}. \tag{6}$$

A common functional form for the shift factor is given by the Arrhenius relationship,

$$a_T = \exp\left[\frac{\Delta H}{R}\left(\frac{1}{T} - \frac{1}{T_0}\right)\right], \tag{7}$$

where ΔH is known as the ''activation energy for flow,''[10] R is the universal gas constant, and T_0 is the reference temperature. For this form, the thermal sensitivity β of the material given in Eq. (2) is given by

$$\beta = \frac{\Delta H}{RT}. \tag{8}$$

Substituting back into Eq. (5), the thermoelastic number becomes

$$\Theta = \frac{R_0}{\lambda(T_0)T_0} \sqrt{\frac{\Delta H}{kR}\frac{1}{a_T}} \sim \sqrt{\frac{1}{a_T}}. \tag{9}$$

Since the shift factor $a_T < 1$ for temperatures $T > T_0$, there is a monotonic increase in the thermoelastic number with increasing temperature. This can be seen clearly by taking the ratio of the value of the thermoelastic numbers for a given fluid and test geometry at any two temperatures:

$$\frac{\Theta(T_{\mathrm{test}})}{\Theta(T_0)} = \sqrt{\frac{a_{T_0}}{a_{T_{\mathrm{test}}}}} = \exp\left[\frac{\Delta H}{2R}\left(\frac{1}{T_0} - \frac{1}{T_{\mathrm{test}}}\right)\right]. \tag{10}$$

As the test temperature is decreased from the reference temperature, the thermoelastic number will decrease and the relative importance of viscous heating compared to elastic effects in the fluid will diminish.

B. Fluid rheology

Two different test fluids are used in these experiments in order to investigate the effects of fluid rheology and thermophysical properties on the elastic flow instability. These viscoelastic fluids consist of 0.05 wt.% solutions of monodisperse polystyrene (PS) (Scientific Polymer Products, Inc.) with a polydispersities of 1.03 and 1.2 and mass-average molecular weights of 6.5×10^6 g/mol (SM2) and 2.0×10^7 g/mol (SM3), respectively. In each case, the polystyrene is dissolved in oligomeric styrene (Hercules Piccolastic) with a molecular weight of $M_w \sim 500$ g/mol. The resulting solutions fall into a class of fluids first described in detail by Boger and co-workers[12] that are highly elastic with an almost constant viscosity. The large viscosities and long relaxation times of these fluids eliminate inertial effects and permit the study of viscoelastic flows at high Deborah numbers.

These two test fluids were initially prepared by Professor Susan J. Muller as part of an interlaboratory comparison of filament stretching rheometers. A detailed analysis of the steady and transient shear and extensional rheology is presented elsewhere.[33] The rheological properties of importance to the present study of elastic flow instabilities will be briefly summarized here and are tabulated in Table III.

In Fig. 3 a master curve of the rheological properties for fluid SM2 at $T_0 = 25\,^{\circ}\mathrm{C}$ is shown, measured with a controlled stress device (TA Instruments, Model AR1000N). A similar master curve can be generated for fluid SM3. The viscoelastic properties of the fluid are characterized in small-amplitude oscillatory shear flow by the dynamic viscosity $\eta'(\omega)$ and the dynamic rigidity $2\eta''(\omega)/\omega \equiv 2G'(\omega)/\omega^2$, which are both functions of the frequency of oscillation. The linear viscoelastic properties are well described by the Rouse–Zimm bead-spring kinetic theory for dilute solutions,[34] as indicated by the solid lines in Fig. 3. Over an intermediate range of frequencies, $1/\lambda_z \ll \omega \ll 1/\lambda_{ps}$, the slope of the dynamic rigidity allows an approximate determination of the hydrodynamic interaction parameter,[35] h^*, which plays a large role in determining the spectrum of relaxation times,[30] given by

TABLE III. Parameters characterizing the viscometric properties of the dilute polystyrene solutions denoted SM2 and SM3.

	Notation	Description	Parameter value SM2	Parameter value SM3
Known:	c	Concentration of high molecular weight polystyrene	0.05%	0.05%
	M_w/M_n	Polydispersity	1.03	1.2
	M_w	Molecular weight (g/mol)	6.5×10^6	2.0×10^7
	$b=L^2$	Extensibility parameter	25000	76700
	T_0	Reference temperature (K)	298	298
Fitted:	η_0	Zero shear rate viscosity (Pa·s)	46.1	55.5
	η_s	Solvent viscosity (Pa·s)	34.0	34.0
	λ_{ps}	Solvent relaxation time (s)	2.7×10^{-4}	2.7×10^{-4}
	h^*	Hydrodynamic interaction parameter	0.15	0.18
	σ_{BD}	Extent of anisotropy in Stokes' law	0.59	0.79
	β_{BD}	Extent of anisotropy in Brownian motion forces	1.0	1.0
Calculated:	$\underline{\lambda}_z$	Zimm (longest) relaxation time (s)	32.1	155
	$\bar{\lambda}$	Oldroyd relaxation time (s)	17.7	81.7
	Ψ_{10}	First normal stress coefficient (Pa·s^2)	428	3510

$$\lambda_j=\frac{\lambda_z}{j^{(2+\sigma)}}, \tag{11}$$

where $\sigma\approx-1.40(h^*)^{0.78}$. The linear viscoelastic moduli can then be conveniently expressed in the following compact form:

$$G'=\frac{c\bar{R}T}{M_w}\sum_{j=1}^{N_m}\frac{(\lambda_z\omega)^2}{j^{2(2+\sigma)}+(\lambda_z\omega)^2}+\frac{\eta_s}{\lambda_{ps}}\frac{(\lambda_{ps}\omega)^2}{1+(\lambda_{ps}\omega)^2}, \tag{12}$$

$$G''=\frac{c\bar{R}T}{M_w}\sum_{j=1}^{N_m}\frac{\lambda_z\omega j^{2+\sigma}}{j^{2(2+\sigma)}+(\lambda_z\omega)^2}+\frac{\eta_s\omega}{1+(\lambda_{ps}\omega)^2}, \tag{13}$$

where N_m is the number of modes used to fit the linear viscoelastic data. In the limit $h^*=0$, the free-draining Rouse model incorporates no hydrodynamic interaction and $2\eta''/\omega\sim\omega^{-3/2}$, whereas in the Zimm (non-free-draining) limit $h^*\approx0.25$ and $2\eta''/\omega\sim\omega^{-4/3}$. At low frequencies ($\omega\leqslant0.01$ rad/s), the fluid is essentially Newtonian with a constant viscosity $\eta_0=\Sigma 1/j^{2+\sigma}c\bar{R}T\lambda_Z/M_w+\eta_s$. However, at high frequencies ($\omega\geqslant1000$ rad/s), the predictions of the Zimm model deviate from the experimental measurements due to the small but finite elasticity of the oligomeric solvent. This additional elasticity can be modeled by an extra Maxwell element for the solvent [the final term in Eqs. (12) and (13)] with a relaxation time $\lambda_{ps}\approx2.7\times10^{-4}$ s, which is in good agreement with the range of values reported by Mackay and Boger.[36] Table III lists the parameters used to compute the material properties for both fluids.

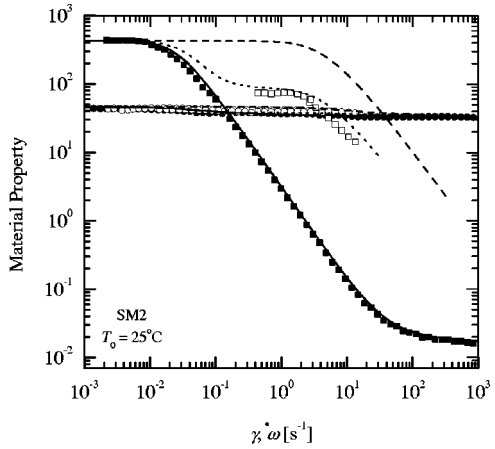

FIG. 3. Rheological material functions of the SM2 fluid. The data include ''○,'' steady shear viscosity $\eta(\dot\gamma)$ (Pa·s); ''●,'' dynamic viscosity $\eta'(\omega)$ (Pa·s); ''■,'' dynamic rigidity $2\eta''(\omega)/\omega$ (Pa·s^2); ''□,'' first normal stress coefficient $\Psi_1(\dot\gamma)$(Pa·s^2); and the corresponding Bird–Deaguiar, FENE-P, and Rouse–Zimm model fits plotted as dotted lines ''- - -,'' dashed lines ''– – –,'' and solid lines ''—,'' respectively.

In steady shear flow, the viscometric properties of the fluids are characterized by the first normal stress coefficient $\Psi_1(\dot\gamma)=[\tau_{11}(\dot\gamma)-\tau_{22}(\dot\gamma)]/\dot\gamma^2$ and viscosity $\eta(\dot\gamma)$, each of which are functions of the shear rate. As shown in Fig. 3, the viscosity of the solution is approximately constant over several decades of shear rate. The fluid is strongly elastic and the first normal stress coefficient shear thins monotonically throughout the entire range over which data can be obtained. By contrast, the Rouse–Zimm bead-spring model predicts a constant value of the first normal stress coefficient as a consequence of the preaveraging of hydrodynamic interactions.[37] The dashed lines in Fig. 3 represent the predictions of a single-mode FENE-P model for the steady shear data. The value of the extensibility parameter, L^2, is derived from molecular quantities for both fluids and can be found in Table III. This value is consistent with measurements of the transient extensional viscosity,[33] but clearly leads to an overprediction of the steady shear properties. An improved description requires a more detailed treatment of hydrodynamic interactions between segments of a polymer chain undergoing a steady shearing deformation. One such model that accounts for the anisotropy in the hydrodynamic drag forces in approximate form is the encapsulated dumbbell model of Bird and DeAguiar.[38] The dotted lines in Fig. 3 represent the predictions of a single-mode Bird–DeAguiar model fit and

are in good agreement with both the viscosity and first normal stress difference measurements of the SM2 fluid. The Bird–DeAguiar model contains two parameters, σ_{BD} and β_{BD}, which specify the extent of anisotropy in the viscous drag on the beads and in the velocity distribution arising from anisotropic Brownian motion, respectively. When $\sigma_{BD}=\beta_{BD}=1$, the FENE-P model is recovered. Our exploratory calculations suggest that to quantitatively describe the viscometric properties of dilute polymer solutions in viscous solvents, the anisotropy in the viscous drag is the primary effect of importance. The Brownian motion of the beads can thus be assumed to be isotropic with $\beta=1$. To determine the proper values of σ_{BD}, the Bird–DeAguiar model was fit to the viscometric properties of the two fluids by minimizes the mean square error between the predicted and computed values of both $\eta(\dot{\gamma})$ and $\Psi_1(\dot{\gamma})$. The results of these fits can be found in Table III.

When defining a Deborah number for reporting the experimental measurements of the critical rotation rate for the onset of the purely elastic instability, a representative measure of the spectrum of relaxation times of the fluid must be chosen. The simplest choice for this fluid time scale is the longest or Zimm relaxation time, λ_Z, determined from the linear viscoelastic measurements and tabulated in Table III. An alternative measure commonly used is the ''average'' or Oldroyd relaxation time, which is a viscosity weighted average of the relaxation spectrum,

$$\bar{\lambda}=\frac{\Psi_{10}}{2\eta_{p,0}}=\frac{\Sigma_{j=1}^{N_m}\eta_j\lambda_j}{\Sigma_{j=1}^{N_m}\lambda_j}. \tag{14}$$

For the Rouse–Zimm spectrum, in which the time constant and viscosity of each relaxation mode is related to the longest mode by a simple recursion relation, this becomes

$$\bar{\lambda}=\frac{\Sigma_{j=1}^{N_m} j^{-2(2+\sigma)}}{\Sigma_{j=1}^{N_m} j^{-(2+\sigma)}}\lambda_z. \tag{15}$$

Theoretical stability analyses[39,40] and scaling arguments[2] show that both the longest and the average value of the relaxation spectrum are important in determining the critical conditions for flow stability.

Even though the shear viscosities of these dilute solutions do not have a strong rate dependence, Fig. 3 demonstrates that, at the shear rates investigated in this research, the first normal stress coefficient shear thins quite heavily. This initial onset of shear thinning is primarily the result of hydrodynamic interaction while more drastic shear thinning at higher shear rates can be attributed to, among other effects, the finite extensibility of the polymer chain. The true relaxation time of the fluid, which can be calculated from the viscometric properties of the fluid previously determined, is thus a strong function of the shear rate,[3]

$$\lambda(\dot{\gamma})\equiv\frac{\Psi_1(\dot{\gamma})}{2\eta_p(\dot{\gamma})}. \tag{16}$$

It has been found in a number of studies of viscoelastic flow instabilities that to achieve quantitative agreement with theoretical predictions it is necessary to use this shear-rate-dependent relaxation time when calculating the effective value of the critical Deborah number for the onset of elastic instabilities.[2,6,39,41] The disadvantage of this approach is that the precise functional form of Eq. (16) becomes model dependent. Therefore, for convenience and clarity the average relaxation time evaluated in the limit of zero shear rate, λ, will be used for reporting critical Deborah numbers unless explicitly indicated otherwise.

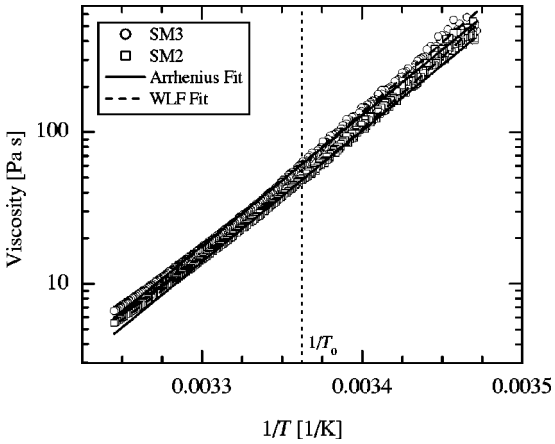

FIG. 4. Steady shear viscosity $\eta(\dot{\gamma})$ as a function of fluid temperature. The data include ''○,'' SM3 test fluid; ''□,'' SM2 test fluid; and the corresponding WLF and Arrhenius model fits plotted as dashed lines ''– – –'' and solid lines ''—'' respectively.

The viscoelastic properties of the test fluids will also change as the temperature of the experiments is varied. In order to compare tests performed at different temperatures, it is necessary to adjust the relaxation time, normal stress difference, and viscosity to their values at a reference temperature of $T_0=25\,^{\circ}\mathrm{C}$. This is accomplished by employing time–temperature superposition with a shift factor $a_T(T,T_0)$ defined in Eq. (6). In this paper we will use the Williams–Landel–Ferry (WLF) equation to specify the functional form of $a_T(T,T_0)$, as it has been found to accurately describe the thermorheological behavior of a wide variety of polymer solutions and melts.[32] However, we will also present results for the Arrhenius formulation of $a_T(T,T_0)$ because of its simplicity and widespread use in previous analyses of flow stability.[17,19,21] The WLF equation has the form[10]

$$\log a_T=\frac{-c_1(T-T_0)}{c_2+(T-T_0)}, \tag{17}$$

where c_1 and c_2 are constants to be determined. Figure 4 demonstrates how the viscosity of the SM2 and SM3 test fluids changes as the temperature is raised from 15 °C to 40 °C. Over the span of 25 °C the zero shear rate viscosity decreases by a factor of 100. Superimposed on these data are fits of the Arrhenius and WLF models for each fluid. The values of the constants used to fit the temperature dependence of the fluid viscosity of both SM2 and SM3 can be found in Table IV. When represented on a semilogarithmic scales of viscosity as a function of $1/T$, the Arrhenius equation [Eq. (7)] predicts a linear relationship that accurately describes the experimental measurements close to the reference temperature T_0. However, the data in Fig. 4 show clear

TABLE IV. Parameters used to describe the temperature dependence of SM2 and SM3 polystyrene solutions with a reference temperature $T_0 = 298$ K.

Notation	Description of parameter	Value of parameter SM2	SM3
c_1	WLF constant	20.1	36.9
c_2	WLF constant (K)	90.4	160
$\Delta H/\tilde{R}$	Arrhenius constant (K)	20 200	19 900

nonlinear trends for large values of $|T-T_0|$ that are better described by the WLF model. For temperatures close to T_0, linearizing the WLF equation [Eq. (17)] suggests $\beta(T_0)=\Delta H/RT_0 \approx c_1 T_0/c_2$. Both the WLF and Arrhenius models predict a thermal sensitivity of $\beta \approx 68$ for both SM2 and SM3. By contrast, the thermal sensitivity is $\beta \approx 20$ for a typical PIB Boger fluid.[42]

The density, thermal conductivity, and heat capacity of fluid SM2 and SM3 can be found in Table V and are assumed to be identical to the thermophysical properties of the oligomeric solvent. Additionally, the properties of both fluids are assumed to be constant over the range of temperatures at which they are tested in this study.[42]

III. EXPERIMENTAL RESULTS

Our goal is to construct an experimental stability diagram such as the one shown in Fig. 2. We first investigate the horizontal (α, De) plane by using the SM3 fluid to perform essentially isothermal experiments, all of which have a thermoelastic number smaller than $\Theta \leqslant 10^{-2}$.

A. Comparison with isothermal theory

The experiments were performed using a controlled stress rheometer (TA Instruments, AR1000N) capable of torque and normal force measurement as well as precise temperature control of the bottom plate using a Peltier device. Each measurement was performed using a fresh sample of Boger fluid. After carefully loading the rheometer, the fluid was allowed to reach thermal and structural equilibrium at a test temperature T before the testing commenced. A constant torque, $\mathcal{T}$, was then applied to the upper fixture. The shear stress acting on the fluid is given by $\tau^{\mathrm{CP}}=3\mathcal{T}/2\pi R_0^3$ for the homogeneous shear flow in the cone-and-plate geometry. For the nonhomogeneous torsional flow in the parallel-plate geometry we report results in terms of the rim shear rate $\dot{\gamma}^{\mathrm{PP}}(r=R_0)=\Omega R_0/h$ and the shear stress at the rim

TABLE V. Thermophysical properties of SM2 and SM3 polystyrene solutions.

Notation	Description of parameter	Value of parameter SM2	SM3
ρ	Density (kg/m^3)	997	997
k	Thermal conductivity (W/m·K)	0.11	0.11
C_p	Heat capacity (J/kg·K)	2.04×10^3	2.04×10^3
α	Thermal diffusivity (m^2/s)	5.4×10^{-8}	5.4×10^{-8}

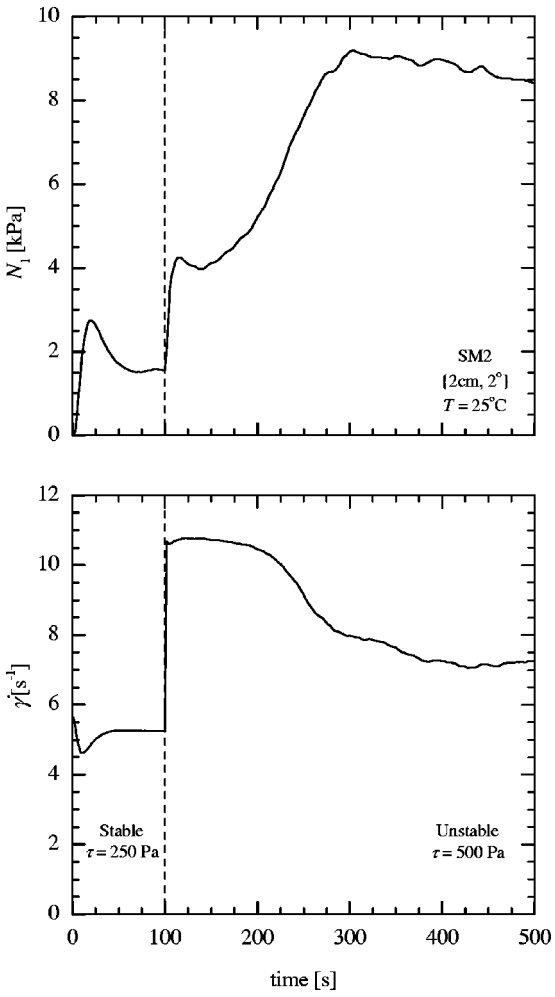

FIG. 5. Transient first normal stress difference and shear rate measurements of the flow between a rotating {2 cm, 2°} cone-and-plate geometry with the SM2 fluid at 25 °C taken at constant applied shear stresses of 250 and 500 Pa.

$\tau^{\mathrm{PP}}(r=R_0)=\mathcal{T}/\pi R_0^3$. The resulting experimentally measured shear rate was averaged over the course of one relaxation time, λ_2, and then compared with subsequent averages until the values were within a $\pm 1\%$ tolerance for two consecutive averages. The fluid was allowed to equilibrate over a maximum period of ten relaxation times, at which point the applied torque was incremented and the fluid was again allowed to reach equilibrium. This protocol was established to ensure that at each test point the fluid microstructure had reached equilibrium. By using a controlled stress device, it is possible to follow the complete flow curve corresponding to the steady two-dimensional base flow and the three-dimensional, time-dependent flow that bifurcates subcritically in the shear rate.[3,4,14] The shear rate is a single-valued function of stress and with careful experimentation it is possible to accurately determine the linear neutral stability condition by identifying the shear rate at which the slope, $d\dot{\gamma}/d\tau$, changes sign.

The time-dependent nature of the purely elastic flow instability is demonstrated in Fig. 5. A constant shear stress is applied to the SM2 test fluid between a rotating cone and plate with $\{R_0,\theta_0\}=\{2\,\mathrm{cm},2°\}$ at a temperature of

$T=25\,^{\circ}\mathrm{C}$ and the resulting shear rate, $\dot{\gamma}$, and first normal stress difference, N_1, are observed over time. At a shear stress of $\tau=250$ Pa ($t<100$ s), the flow is stable, exhibiting an initial overshoot and then becoming steady in time. After 100 s, the shear stress is increased to a value of $\tau=500$ Pa. Subsequent measurements of normal stress and shear rate deviate sharply from the expected equilibrium values and do not reach a steady state, but instead demonstrate the time-dependent behavior and apparent antithixotropy seen in previous studies.[3,14] The duration of this experiment was chosen to be much larger than both the polymer relaxation time ($\lambda_z \cong 32$ s) and the time scale for thermal diffusion is ($t_{\text{thermal}} \cong 9$ s) to ensure that kinematic and thermal equilibrium were achieved. A more detailed discussion of the importance of test protocol can be found in Sec. III C.

In Fig. 6, the experimental results for the SM3 Boger fluids at very low Nahme number, $\mathrm{Na} \leqslant 10^{-3}$, are compared with the multimode isothermal linear stability analysis of Avagliano and Phan-Thien.[43] The experimentally observed critical Deborah number is presented both as the product of the angular frequency and the average relaxation time, $\bar{\lambda}$, evaluated in the limit of zero shear rate and as the product of the angular rotation rate and the shear-rate-dependent relaxation time, $\lambda(\dot{\gamma})$. As noted in Table I, when the free surface effects in the parallel-plate geometry are considered at small aspect ratios, the linear stability theory predicts that the critical Deborah number for the onset of the elastic instability should have a linear dependence on aspect ratio.[6,43] Through careful experimental techniques, McKinley *et al.*[3] were able to very closely approach the linear neutral stability condition and minimize the amplitude of the disturbance, which for a subcritical Hopf bifurcation must be finite. In fact, both Öztekin *et al.*[44] and Avagliano and Phan-Thien[43] were able to quantitatively match their linear stability analysis predictions to the experimental neutral stability data of McKinley *et al.*[3] The solid line in Fig. 6 is the linear stability analysis provided by Avagliano for the multimode Rouse–Zimm spectrum of fluid SM3. Although neither value of the critical Deborah number quantitatively matches the theory over the entire range of aspect ratios tested, both measures demonstrate the predicted linear dependence on aspect ratio. The stability locus for the multimode model was calculated using the approximation proposed by McKinley *et al.*,[2]

$$\left(\frac{\mathrm{De}_{\text{multimode}}}{\mathrm{De}_{\text{single mode}}}\right)_{\text{crit}} \approx \left[\frac{\sum_{j=1}^{n} \frac{\lambda_j U}{R_c}\frac{\tau_{11j}}{\eta_0\dot{\gamma}}}{\frac{\bar{\lambda} U}{R_c}\frac{\tau_{11}}{\eta_0\dot{\gamma}}}\right]^{1/2}, \tag{18}$$

where U is the local velocity along a streamline with radius of curvature R_c. The tensile stress along the streamline for each mode is τ_{11j} and the local shear rate is $\dot{\gamma}$. Calculations show that this equation allows one to estimate the results for the analysis of any multimode spectrum from the results of a single-mode analysis to within ten percent of the true value.[43] For torsional flows in the parallel plate geometry, Equation (18) can be simplified by substituting $U=r\Omega$, $R_c=r$, $\tau_{11j}=2cRT\lambda_j^2\dot{\gamma}^2/M_w$, and $\dot{\gamma}=\Omega/\alpha$ to yield

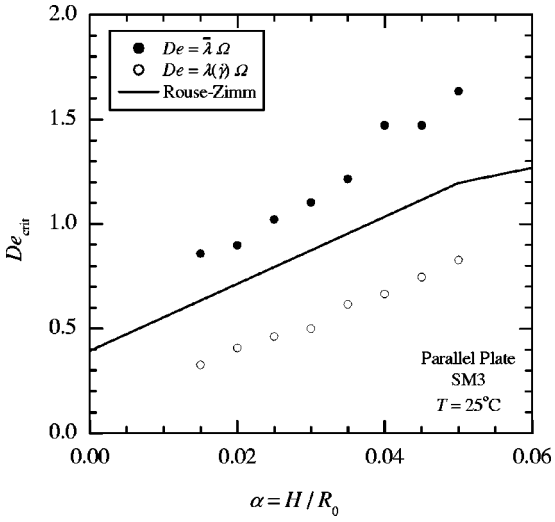

FIG. 6. Effect of aspect ratio on the critical Deborah number for the onset of the purely elastic flow instability between a rotating parallel plate for the SM3 test fluid at 25 °C.

$$\left(\frac{\mathrm{De}_{\text{multimode}}}{\mathrm{De}_{\text{single mode}}}\right)_{\text{crit}} \approx \frac{\lambda_{\text{rms}}}{\bar{\lambda}}, \tag{19}$$

where

$$\lambda_{\text{rms}} = \left(\frac{\sum_{j=1}^{N_m} \eta_j \lambda_j^2}{\sum_{j=1}^{N_m} \eta_j}\right)^{1/2}. \tag{20}$$

The predictions of the isothermal linear stability analysis for flow in a rotating cone and plate have also been compared against experimentally determined critical conditions for both the SM2 and SM3 fluids in other geometries with $\{R_0, \theta_0\}=\{3\text{ cm},1^{\circ}\}$, $\{2\text{ cm}, 2^{\circ}\}$, and $\{1\text{ cm}, 4^{\circ}\}$. These tests were performed at low temperatures and vanishingly small Nahme numbers, $\mathrm{Na} \leqslant 10^{-3}$. The results of these tests can be found in Fig. 7. The experimental and theoretical critical Deborah numbers are presented as the product of the critical angular frequency and the average or Oldroyd relaxation time evaluated in the limit of zero shear rate, $\mathrm{De}=\bar{\lambda}\Omega$. The predictions of the FENE-PM and the Bird–DeAguiar models, computed using the scaling approach discussed by McKinley *et al.*,[2] are presented along with the Rouse–Zimm multimode analysis. Recalling the results of the linear stability theory of Olagunju.[26] presented in Table I, one expects the critical Deborah number for the onset of the elastic instability to scale with the square root of the cone angle and to appear as a straight line in Fig. 7. As one quickly observes, this is only true for the shear-rate-independent Rouse–Zimm model. The modifications to the multimode FENE-PM curve, the Bird–DeAguiar curve, and the experimental data at small cone angles are the result of the shear-rate dependence of the viscometric properties caused by the polymer's finite extensibility[3] and by hydrodynamic interactions.[38] For very small cone angles, the shear rate at the onset of instability is very high and the true relaxation time of the fluid is much smaller than the Oldroyd relaxation time used in the formulation of the Deborah number. For example, choosing a moderately large cone angle of $\theta_0^{1/2}=0.5$ ($\theta_0 \cong 14^{\circ}$), which for

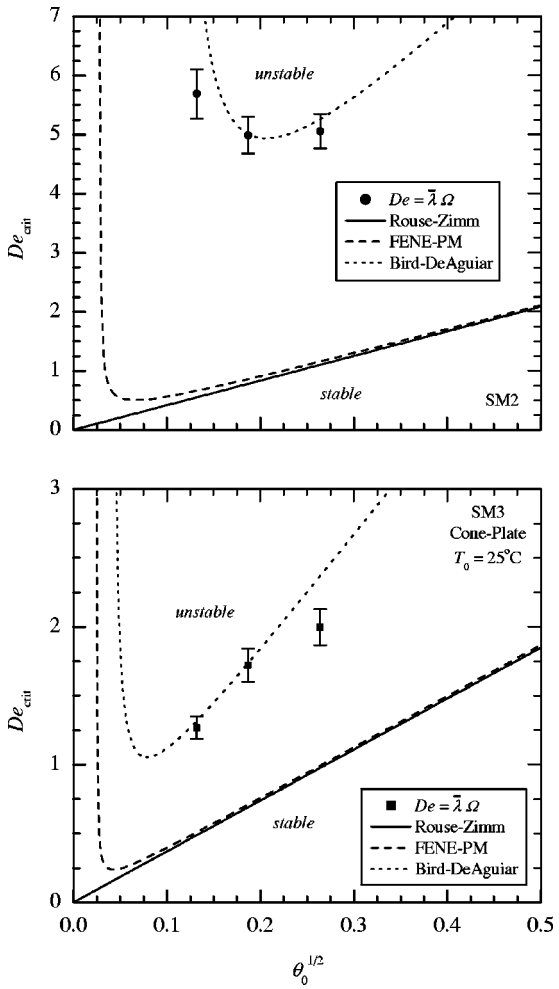

FIG. 7. The effect of the cone angle on the critical Deborah number for the onset of the purely elastic flow instability between a rotating cone and plate for the (a) SM2 and (b) SM3 test fluids.

the SM2 fluid and the Rouse–Zimm model corresponds to a critical Deborah number of $\mathrm{De}_{\mathrm{crit}}=2.08$, results in a critical shear rate of $\dot{\gamma}_{\mathrm{crit}}=\mathrm{De}_{\mathrm{crit}}/(\theta_0\lambda_{\mathrm{SM2}})=0.47\,\mathrm{s}^{-1}$. It is clear from Fig. 3 that an appreciable decrease in the fluid elasticity has already occurred at this shear rate. A quantitative agreement can only be achieved when evaluating the critical Deborah number with the (constant) average relaxation time, $\bar{\lambda}$, provided the constitutive model accurately represents the viscometric properties of the fluid. This requirement can be clearly seen in Fig. 7 by examining the two broken lines that represent the stability boundaries for the FENE-PM and Bird–DeAguiar models. The FENE-PM model qualitatively captures the onset of shear thinning in $\Psi_1(\dot{\gamma})$ at very high shear rates (low cone angles) but seriously overpredicts the fluid elasticity at intermediate shear rates, as shown in Fig. 3. By contrast, the Bird–DeAguiar model captures, at least semiquantitatively, the decrease in $\Psi_1(\dot{\gamma})$ arising from hydrodynamic interactions and much more accurately predicts the observed stability boundaries.

Although it cannot be seen in Fig. 7, at low enough shear rates (high enough cone angles), the Bird–DeAguiar model does asymptotically approach the Rouse–Zimm stability curve. Without continuing the abscissa of Fig. 7 to large cone angles, we can easily validate this statement by inspecting the viscometric data presented in Fig. 3. The Bird–DeAguiar model satisfies simple fluid theory, and so, in the limit of low shear rates, the rate-dependent relaxation time of the model will become constant and equal to the rate-independent relaxation time of the Rouse–Zimm model. However, at these rates ($\dot{\gamma}\leqslant 10^{-2}\,\mathrm{s}^{-1}$) the cone angles required ($\theta_0\geqslant 170\,\mathrm{rad}$) would be completely unphysical.

If the shear-rate-dependent relaxation time is used in the formulation of the critical Deborah number, $\mathrm{De}=\lambda(\dot{\gamma})\Omega$, instead of the Oldroyd relaxation time, all three models will follow the same square root dependence on cone angle as the shear-rate-independent Rouse–Zimm model in Fig. 7. If the experimental measurements of the critical rotation rate are also reported as a critical value of the shear-rate-dependent Deborah number [using Eq. (16) to compute the relaxation time], quantitative agreement with all three of the models can be obtained. This lends additional credence to the use of the shear-rate-dependent relaxation time when comparing experiments with linear stability theory[2,6,41] and is the only way to accurately fit the neutral stability data if the viscometric data of the viscoelastic test fluid cannot be accurately modeled by the chosen constitutive equation.

B. Nonisothermal modifications to stability of elastic torsional flow

If Eq. (9) is evaluated for fluid SM2 in the {2 cm, 2°} cone-and-plate geometry, the thermoelastic number becomes

$$\Theta_{\mathrm{SM2}}=\frac{1}{\sqrt{a_T}}\frac{R_0}{\bar{\lambda}(T_0)}\sqrt{\frac{\eta_0(T_0)\beta(T_0)}{kT_0}}=\frac{0.011}{\sqrt{a_T}}. \tag{21}$$

For temperatures greater than the reference temperature $T>T_0$, the shift factor is smaller than 1 and the thermoelastic number Θ will increase. We show below that when the thermoelastic number is equal to $\Theta\approx 0.061$ ($T\approx 43\,^{\circ}\mathrm{C}$), viscous heating results in significant modifications to the flow stability curves. For temperatures less than the reference temperature $T<T_0$, the shift factor $a_T>1$ and the thermoelastic number decreases, lowering the slope of the trajectory followed by experiments in the three-dimensional space shown in Fig. 2.

Similar calculations of the thermoelastic number for fluids SM3 and SM1 described by Anna *et al.*[33] show that $\Theta_{\mathrm{SM3}}=0.0024a_T^{-1/2}$ and $\Theta_{\mathrm{SM1}}=0.092a_T^{-1/2}$. Viscous heating is therefore not important until temperatures of $T\approx 70\,^{\circ}\mathrm{C}$ for fluid SM3, while it is important for all temperatures greater than $T\gtrsim 10\,^{\circ}\mathrm{C}$ for fluid SM1. Indeed, experiments with fluid SM1 showed no elastic instability for any temperatures or shear rates studied. Fluid SM2 was thus chosen for the nonisothermal tests described below because its thermophysical properties allow for excellent control of the purely elastic instability at reasonable temperatures and cone angles.

Using the same testing protocol outlined in the previous section, the effect of viscous heating was systematically examined by performing torque sweeps on the SM2 fluid in the cone-and-plate geometry over a wide range of temperatures $15\,^{\circ}\mathrm{C}\leqslant T\leqslant 50\,^{\circ}\mathrm{C}$. In Fig. 8, we show the form of the flow

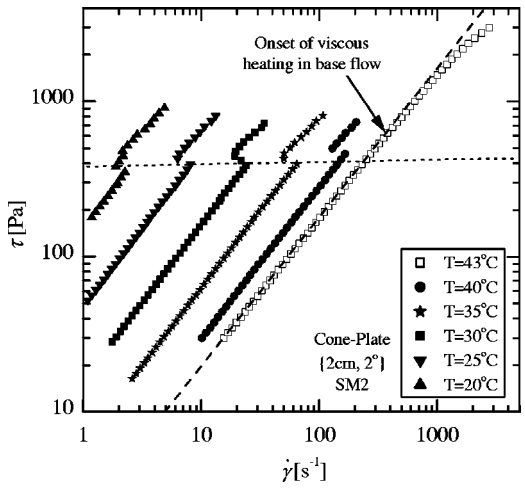

FIG. 8. The onset of an elastic flow instability as observed in shear stress sweeps of the SM2 test fluid at various temperatures using the {2 cm, 2°} cone-and-plate geometry.

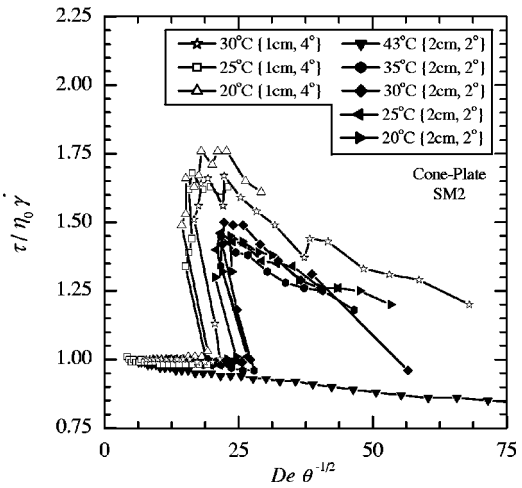

FIG. 9. Normalized shear stress as a function of the linear stability control parameter De $\theta^{-1/2}$.

transition for fluid SM2 using a cone-and-plate geometry with $\{R_0, \theta_0\} = \{2\text{ cm}, 2°\}$. As observed by Magda and Larson[14] and by McKinley *et al.*,[3] the instability is subcritical in the shear rate. At a temperature of 43 °C, a strong deviation in the shear stress from a linear dependence on shear rate indicates the onset of viscous heating in the sample. Simultaneous measurement of the first normal stress difference shows that there is an even more dramatic loss of elasticity, as is shown in Fig. 11. The result is a drastic reduction in the shear-rate-dependent relaxation time and, consequently, a failure to reach the critical conditions for the onset of the elastic instability.

In the isothermal linear stability theory, the critical Deborah number for the onset of the purely elastic flow instability is determined to be a constant, independent of temperature (see Table I). When represented in terms of dimensional parameters, time–temperature superposition of the material properties leads to a linear dependence of the critical flow conditions on the test temperature. If the stability theory is expressed in terms of a critical shear stress, one obtains

$$\tau_{\text{crit}} \equiv \eta \dot{\gamma}_{\text{crit}} = \frac{\eta}{\lambda}\left(\frac{\overline{\lambda\Omega}_{\text{crit}}}{\theta_0}\right). \tag{22}$$

Substituting Eq. (6) into Eq. (22) one finds that the critical shear stress varies linearly with temperature,

$$\tau_{\text{crit}}(T) = \tau_{\text{crit}}(T_0)\,\frac{T}{T_0}, \tag{23}$$

where $\tau_{\text{crit}}(T_0)$ is the critical stress for the onset of instability at the reference temperature, T_0. The dotted line in Fig. 8 represents the prediction of Eq. (23) for the critical shear stress. This decoupled isothermal approximation correctly predicts the weak modulation in the critical conditions for the onset of instability at low thermoelastic numbers, but does not take into account the strong coupling that arises at large thermoelastic numbers.

The data in Fig. 8 can be collapsed by plotting the measured shear stress nondimensionalized by the shear stress expected for the steady base flow, $\eta_0 \dot{\gamma}$, against the control parameter expected from the linear stability theory, $\text{De}/\theta_0^{1/2}$.[26] In Fig. 9, we plot the stability data for both the {1 cm, 4°} and the {2 cm, 2°} cone-and-plate geometries for the SM2 fluid over a wide range of temperatures. Although the data from the two cone angles do not superimpose exactly, the general agreement is very good. If the shear-rate-dependent relaxation time is used in the formulation of the Deborah number, the results for different cone angles would very nearly superimpose. The data show that increasing the temperature of the test fluid, and thus the Nahme number, delays the onset of the purely elastic flow instability, but has little effect on the amplitude of the fully developed time-dependent nonlinear state until the thermoelastic number approaches its critical value. At that point, the instability is completely suppressed by viscous heating. This transition happens over a very small range of temperatures ($37\,°\text{C} \leqslant T \leqslant 43\,°\text{C}$) and we now proceed to study this region in more detail.

To highlight the effect of viscous heating on the base flow, in Fig. 10 we show the progressive variation in the dimensionless time scale for viscous heating, $\text{Na}^{1/2} = t_{\text{heat}}\dot{\gamma}$, against the dimensionless viscoelastic time scale, De, for fluid SM2 in the {2 cm, 2°} cone-and-plate rheometer as the deformation rate is increased. The filled symbols in Fig. 10 represent steady two-dimensional flow while hollow symbols represent the unstable regime. A dashed line denoting the neutral stability curve has been superimposed on the data to guide the reader's eye, but is not meant to be inferred as quantitative. At very low Nahme numbers, viscous heating is not significant and the resulting delay in the onset of the elastic instability, although clearly evident, is quite small and in agreement with Eq. (23). At a temperature of 40 °C, viscous heating begins to strongly stabilize the flow, shifting the onset of the instability upward to a Deborah number that is 15% above the value obtained at a low Nahme number. When the temperature is increased still further to 43 °C, the

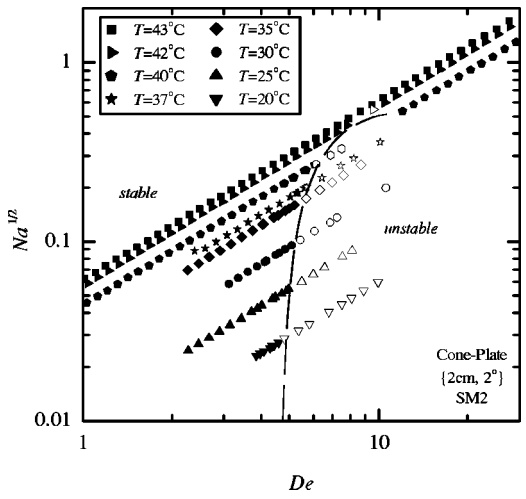

FIG. 10. Stability diagram for the flow between a rotating {2 cm, 2°} cone-and-plate geometry. As the Deborah number is increased, the flow goes from stable flow conditions represented by filled symbols ''●'' to unstable flow conditions represented by hollow symbols ''○.''

flow becomes stable at all shear rates. At this temperature, the critical thermoelastic number is $\Theta_{crit}=0.061$ corresponding to $Na_{crit}^{1/2}=0.45$ and $De_{crit}=7.3$. In order to obtain quantitative agreement with the results of linear stability analyses, it is necessary to report values of critical conditions in terms of the shear-rate-dependent relaxation time, $\lambda(\dot{\gamma})$, rather than the average relaxation time, λ. If the fluid properties (in particular, the fluid relaxation time) are allowed to vary with shear rate, the critical thermoelastic number increases by more than an order of magnitude to a value very close to one $\Theta_{crit}(\dot{\gamma})=0.92$.

The coupling of viscous heating effects and the onset of flow instability is also manifested in a profound way in the normal stress data. We show in Fig. 11 the shear stress and first normal stress difference as a function of shear rate for torque sweeps performed with the {2 cm, 2°} cone-and-plate rheometer on the SM2 fluid for temperatures of 40 °C, 42 °C, and 43 °C. As the temperature is increased from 40 °C to

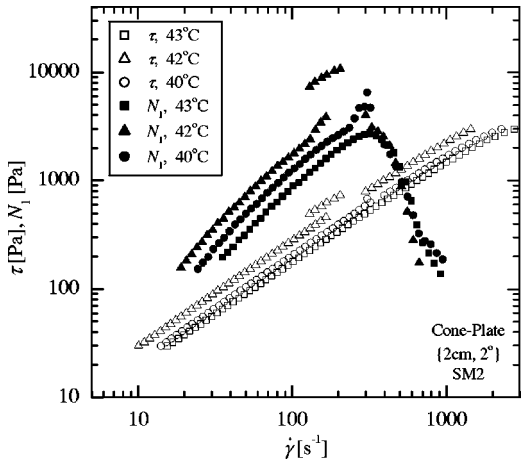

FIG. 11. Viscometric properties for flow of SM2 fluid between a rotating {2 cm, 2°} cone-and-plate geometry at three temperatures showing the effect of viscous heating on the purely elastic flow instability.

43 °C, the magnitude and duration of the elastic instability is diminished while the onset is delayed to a larger critical Deborah number by viscous heating. The onset of viscous heating is characterized by a sharp decrease in the first normal stress difference and is differentiable from simple shear thinning by the nonmonotonic nature of the curves. This can be seen most clearly in measurements of the shear stress and first normal stress difference taken at 43 °C. At low shear rates $\dot{\gamma}\lesssim 60\,s^{-1}$ (Na≈0.008), the viscometric data is consistent with the predictions of the Rouse–Zimm and Bird–DeAguiar models. A maximum in the shear stress corresponding to a ''thermal blowup'' is reached at a shear rate of $\dot{\gamma}\approx 2700\,s^{-1}$ (Na≈12). In a controlled stress experiment, no steady values of the shear rate above this maximum shear stress are attainable.[42] The first normal stress difference also goes through a local maximum, but at a much lower shear rate $\dot{\gamma}\approx 320\,s^{-1}$ (Na≈0.17). This degradation of fluid elasticity results in the complete suppression of the elastic flow instability. In the experiments at 40 °C and 42 °C, the flow becomes unstable before viscous heating can begin to significantly degrade the elasticity. However, the instability is quickly suppressed after a critical value of the Nahme number $Na_{crit}\approx 0.23$ is reached. The shear stress does begin to show noticeable nonlinear effects at these moderate shear rates, but the normal stress is clearly a much better indicator of viscous heating. These viscous heating trends are in excellent agreement with the recent measurements of similar polystyrene- and polyisobutylene-based Boger fluids performed by Arigo.[42]

C. Effect of test protocol on stability observations

Since there are a number of important time scales characterizing different physical processes in the fluid (see Table I), the choice of experimental test protocol and the associated observation window can have a significant impact on the observed results of the experiments. Theoretical stability analyses[19,21] of nonisothermal viscoelastic flows assume that the base flow on to which perturbations are imposed is steady and fully developed. For the cone-and-plate geometries the timescale for thermal diffusion is $5\,s\lesssim t_{thermal}\lesssim 10\,s$ (depending on cone geometry) and the time scale for the stress to reach steady state is $\lambda_z(T_0)=31.1\,s$. If the experiment ramps in torque are imposed too quickly, then the fluid may not be able to reach thermal or structural equilibrium, resulting in the observation of a pseudosteady state, which is, in fact, dependent on the speed at which one probes the material. The issue of structural equilibrium is most pertinent at low temperatures where the relaxation time is much longer than the time scale for thermal diffusion. Ramping the torque too quickly at low temperatures will result in the observation of a critical Deborah number much higher than expected because the fluid stresses will not be fully developed. At higher temperatures, the relaxation time, $\lambda(T)=\lambda_z(T_0)/a_T$, decreases rapidly and it is the thermal diffusion time that becomes important.

When both scales are equally important, very complex dynamics may ensue. In Fig. 12, we show measurements of the SM2 fluid in a cone-and-plate geometry with

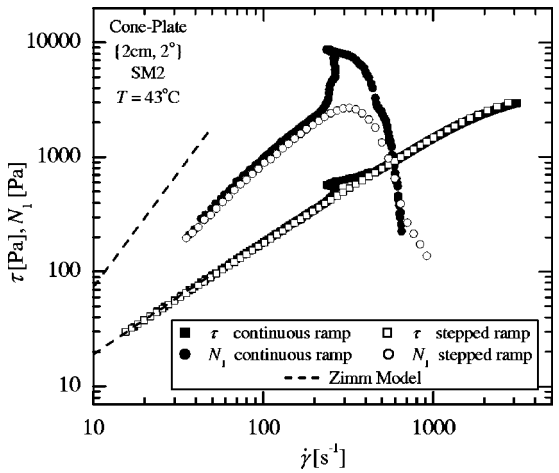

FIG. 12. Viscometric properties for flow of SM2 fluid between a rotating {2 cm, 2°} cone-and-plate geometry at $T=40\,^{\circ}\mathrm{C}$, showing the effect of test protocol. The predictions of the Rouse–Zimm bead spring model are plotted as dashed lines ''– – –'' for low shear rates.

$\{R_0,\theta_0\}=\{2\ \mathrm{cm},\ 2^{\circ}\}$ at a test temperature of $T=43\,^{\circ}\mathrm{C}$. On the basis of the steady-state experiments described in Sec. III B, using step changes in the applied shear stress and a ten relaxation time observation window, viscous heating is found to completely stabilize the flow. The corresponding data for the shear stress and normal stress are shown as open symbols. As the shear rate increases, viscous heating results in an apparent shear thinning in the shear stress and a dramatic decrease in the normal force exerted on the cone. However, if a continuous stress ramp with rate of increase of $d\tau/dt=5$ Pa/s is imposed, the data corresponding to the filled symbols is obtained and the flow appears to exhibit an elastic instability. When the underlying steady one-dimensional shear flow is stable ($\dot{\gamma}\leqslant 110\ \mathrm{s}^{-1}$), the two curves closely parallel each other and the shear stress predictions of the Rouse–Zimm bead spring model. The departure in the first normal stress data from the predictions of the quasilinear Rouse–Zimm model is the result of shear thinning caused by hydrodynamic interactions and can be captured by the Bird–DeAguiar model. At higher shear rates, a transient subcritical instability is observed. As the stress is increased, the shear rate initially decreases and the normal stress increases dramatically, as previously observed in Fig. 11 for lower test temperatures. However, as the thermal profile in the fluid begins to develop through the rapid azimuthal, and slower radial, diffusion of thermal energy, the effective elasticity of the fluid decreases. Eventually, the instability is effectively eliminated and the shear rate returns to a steady, stable value monotonically increasing with the imposed stress.

IV. CONCLUSIONS

In this study, we have systematically demonstrated the importance of nonisothermal flow effects on the stability of torsional flows of highly elastic polymer solutions. Two monodisperse polystyrene test fluids of different molecular weight have been used to investigate the role of the fluid rheology. The agreement with isothermal linear stability analyses for the Rouse–Zimm and Bird–DeAguiar constitutive models in both cone-and-plate and parallel-plate geometries was found to be good, especially if shear thinning in the fluid relaxation time is accounted for. It was then shown that the proper dimensionless groups to consider when investigating purely elastic instabilities in viscoelastic flows are the Deborah number and the thermoelastic number $\Theta=\mathrm{Na}^{1/2}/\mathrm{De}$, which measures the importance of coupling between the fluid elasticity and the nonlinearities arising from viscous heating. The thermoelastic number can be influenced by changes in geometry, molecular weight, and temperature. By varying the ambient temperature of the test fluid through a fairly narrow range, it was possible to progressively delay the onset of the purely elastic flow instability through a decrease in elasticity caused by temperature gradients across the gap. At thermoelastic numbers greater than $\Theta>\Theta_{\mathrm{crit}}\approx 0.062$, the flow instability can be eliminated entirely by the same mechanism.

When the effects of energetics on the linear stability of the viscoelastic flow within a Taylor–Couette device were investigated by Al-Mubaiyedh *et al.*,[21] a new mode of different spatiotemporal character to the mode arising from isothermal linear stability analysis was predicted to be the most unstable. The critical conditions for onset of this new stationary mode of instability are much lower than those required for the isothermal mode and are also in better agreement with the experimental observations. By contrast, in earlier investigations of the viscoelastic torsional flow between a rotating cone and plate or between two coaxial parallel plates, the critical conditions for the onset of spiral secondary flows were observed to be consistent with the predictions of isothermal linear stability analysis.[3,4,27] This has been confirmed by our present experiments when the thermoelastic number is small. No new mode of instability is observed and viscous heating effects (corresponding to an increasing thermoelastic number) are found to progressively stabilize the subcritical bifurcation. These two studies thus do not appear to be consistent. However, very recently, Al-Mubaiyedh *et al.*[45] extended their linear stability analysis of nonisothermal viscoelastic flows to the case of pressure-driven Taylor–Dean flow. In this geometry they found that, as in the present torsional flow experiments, the dominant mode of the instability does not change with the addition of viscous heating, but is instead dramatically stabilized. The thermal mode is still present, but is not the dominant mode until $\mathrm{Pe}\gg 1$.

The differences observed between the stability characteristics of viscoelastic flow in the Taylor–Couette, Taylor–Dean, and torsional geometries must be the result of differences in the symmetries of the base velocity, temperature, and stress fields. When the temperature at both walls is the same and the fluid is heated through viscous dissipation, the local fluid temperature achieves a maximum at the center of the gap. It is easy to physically understand how viscous heating can stabilize any of these flows. As discussed in McKinley *et al.*,[2] purely elastic instabilities arise from an interplay between streamline curvature and elastic normal stresses. When a critical Deborah number is reached, the following dimensionless parameter exceeds a critical value:

$$\left(\frac{\lambda U}{R_c}\frac{\tau_{11}}{\eta_0\dot{\gamma}}\right)^{1/2} \geqslant M_{\text{crit}}, \tag{24}$$

and the flow becomes unstable. The temperature increase caused by viscous heating leads to a decrease of both the viscosity and the elasticity of the test fluid and thus results in a decrease in the elastic hoop stress. The critical condition expressed in Eq. (24) is no longer exceeded along local streamlines, even though the critical conditions would have been reached globally for an isothermal flow at the same rate. This thermoelastic mechanism has been found to stabilize the isothermal elastic modes of all the flows examined, including the Taylor–Couette geometry for $\text{Pe}<10^4$.[21]

In the base flow of the Taylor–Couette geometry the shear stress is uniform across the gap. Viscous heating breaks the base flow symmetry in the gradient direction. A new temporal mode of instability is caused by radial convection of thermal gradients across streamlines. It appears that the symmetry of the base stress field in Taylor–Couette flow may shift the onset of this new thermoelastic instability to much smaller Peclet numbers ($\text{Pe}\gtrsim 10^4$), than is found in the case of Taylor–Dean flow ($\text{Pe}\gtrsim 10^5$), in which the base-state stress field is already inhomogeneous.[21,45]

If one applies this same reasoning to the two torsional flow geometries, then one would expect that because of the homogeneity of the stress field in the base state of the cone-and-plate geometry, the effect of viscous heating should lead to a new mode of instability, as observed in the linear stability calculations for the Taylor–Couette geometry. By contrast, one would reason that the parallel-plate geometry, in which the stress field is already radially inhomogeneous, would more closely resemble the Taylor–Dean flow geometry. However, these symmetry arguments do not agree with our experimental observation. Viscometric flow in the cone-and-plate geometry does not appear to exhibit a new mode of instability when viscous heating is included, but rather only a stabilization of the isothermal elastic spiral instability. The magnitude of viscous heating in a flow scales with the Nahme number, which for the cone-and-plate geometry can be written as $\text{Na}=\beta r^2\Omega^2/kT_0$. Thus, even though the shear rate, $\dot{\gamma}=\Omega/\theta_0$, is constant in the cone-and-plate geometry, the velocity, and the resulting viscous dissipation, increases radially. Therefore, unlike the Taylor–Couette geometry, viscous heating results in nonhomogeneous temperature variations in both the gradient and the neutral direction for the cone-and-plate geometry. In the parallel-plate geometry the gap between the plates is constant, but both the temperature field and shear rate (or in dimensionless terms, the Nahme–Griffiths number and the Weissenberg number, respectively) will exhibit radial variations. The two torsional flows thus seem to have more in common with the Taylor–Dean geometry. Such base flow symmetry arguments may help to rationalize these differences in thermoelastic effects, however, what is ultimately required is a detailed comparison of the linearized disturbance equations for viscoelastic flow in the Taylor–Couette, Dean, and torsional flow geometries.

The subcritical bifurcation in shear rate observed in the present experiments is different from the turning point in the shear stress—shear rate curve corresponding to the ''thermal blowup'' seen in similar Boger fluids and highly viscous Newtonian fluids[42] at large Nahme numbers. This instability, which can be seen in both the shear stress and the normal stress data presented in Fig. 11 at $T=43\,^{\circ}\text{C}$, corresponds to the point at which viscous heating reduces the viscosity so significantly that increases in applied shear rate result in a decrease of the measured shear stress necessary to drive the flow.[17]

The effects of viscous heating will always be present to some extent in the shear flow of highly elastic fluids. These effects will be especially important in shear flows with closed streamlines in which the heat from viscous dissipation can be accumulated in the device over long periods of times. In this work, we have shown that the effect of viscous heating can be minimized by considering the functional dependence of the thermoelastic parameter in Eq. (5) and by decreasing the ambient temperature of the test or by utilizing small devices. Such an approach has been used to minimize thermal noise in detailed studies of other hydrodynamic flow instabilities.[46]

ACKNOWLEDGMENTS

The authors wish to acknowledge financial support from The Lord Foundation and from NASA under Grant No. NCC3-610, Professor Susan Muller for supplying the fluids used in this paper, Dr. Shelley Anna for performing the initial rheological characterization of the fluids, and Dr. Aaron Avagliano for providing the isothermal linear stability analysis of the parallel-plate geometry.

[1] R. G. Larson, E. S. G. Shaqfeh, and S. J. Muller, ''A purely elastic instability in Taylor–Couette flow,'' J. Fluid Mech. **218**, 573 (1990).
[2] G. H. McKinley, P. Pakdel, and A. Oztekin, ''Rheological and geometric scaling of purely elastic flow instabilities,'' J. Non-Newtonian Fluid Mech. **67**, 19 (1996).
[3] G. H. McKinley, J. A. Byars, R. A. Brown, and R. C. Armstrong, ''Observations on the elastic instability in cone-and-plate and parallel-plate flows of polyisobutylene Boger fluid,'' J. Non-Newtonian Fluid Mech. **40**, 201 (1991).
[4] D. O. Olagunju, ''Elastic instabilities in cone-and-plate flow: Small gap theory,'' Z. Angew. Math. Phys. **46**, 946 (1995).
[5] D. O. Olagunju, ''Effect of free surface and inertia on viscoelastic parallel plate flow,'' J. Rheol. **38**, 151 (1994).
[6] A. Avagliano and N. Phan-Thien, ''Torsional flow: elastic instability in a finite domain,'' J. Fluid Mech. **312**, 279 (1996).
[7] C. J. S. Petrie and M. M. Denn, ''Instabilites in polymer processing,'' AIChE J. **22**, 209 (1976).
[8] R. G. Larson, ''Instabilities in viscoelastic flows,'' Rheol. Acta **31**, 213 (1992).
[9] E. S. G. Shaqfeh, ''Purely elastic instabilities in viscometric flows,'' Annu. Rev. Fluid Mech. **28**, 129 (1996).
[10] R. B. Bird, R. C. Armstrong, and O. Hassager, *Dynamics of Polymeric Liquids: Volume 1 Fluid Mechanics* (Wiley, New York, 1987).
[11] H. H. Winter, ''Viscous dissipation in shear flows of molten polymers,'' Adv. Heat Transfer **13**, 205 (1977).
[12] D. V. Boger, ''A highly elastic constant-viscosity fluid,'' J. Non-Newtonian Fluid Mech. **3**, 87 (1977/78).
[13] M. J. MacDonald and S. J. Muller, ''Shear rheology of polymer solutions near the critical condition for elastic instability,'' Rheol. Acta **36**, 97 (1997).
[14] J. J. Magda and R. G. Larson, ''A transition occurring in ideal elastic liquids during shear flow,'' J. Non-Newtonian Fluid Mech. **30**, 1 (1988).
[15] B. Yesilata, A. Oztekin, and S. Neti, ''Non-isothermal viscoelastic flow

through an axisymmetric sudden contraction,'' J. Non-Newtonian Fluid Mech. **89**, 133 (2000).
[16]K. Kunisch and X. Marduel, ''Optimal control of non-isothermal viscoelastic fluid flow,'' J. Non-Newtonian Fluid Mech. **88**, 261 (2000).
[17]C.-S. Yueh and C.-I. Weng, ''Linear stability analysis of plane Couette flow with viscous heating,'' Phys. Fluids **8**, 1802 (1996).
[18]T. C. Ho, M. M. Denn, and B. E. Anshus, ''Stability of low Reynolds number flow with viscous heating,'' Rheol. Acta **16**, 61 (1977).
[19]L. E. Becker and G. H. McKinley, ''The stability of viscoelastic creeping plane shear flows with viscous heating,'' J. Non-Newtonian Fluid Mech. **92**, 109 (2000).
[20]B. M. Baumert and S. J. Muller, ''Flow regimes in model viscoelastic fluids in a circular Couette system with independently rotating cylinders,'' Phys. Fluids **9**, 566 (1997).
[21]U. A. Al-Mubaiyedh, R. Sureshkumar, and B. Khomami, ''Influence of energetics on the stability of viscoelastic Taylor–Couette flow,'' Phys. Fluids **11**, 3217 (1999).
[22]N. Phan-Thien, ''Coaxial-disk flow of an Oldroyd-B fluid: Exact solution and stability,'' J. Non-Newtonian Fluid Mech. **13**, 325 (1983).
[23]N. Phan-Thien, ''Cone-and-plate flow of the Oldroyd-B fluid is unstable,'' J. Non-Newtonian Fluid Mech. **17**, 37 (1985).
[24]D. O. Olagunju and L. P. Cook, ''Secondary flows in cone and plate flow of an Oldroyd-B fluid,'' J. Non-Newtonian Fluid Mech. **46**, 29 (1993).
[25]D. O. Olagunju, ''On short wave elastic instabilities in parallel plate flow,'' *Proceedings of the 1997 ASME Annual Meeting*, 1997.
[26]D. O. Olagunju, ''Hopf bifurcation in creeping cone-and-plate flow of a viscoelastic fluid,'' Z. Angew. Math. Phys. **48**, 361 (1997).
[27]G. H. McKinley, A. Oztekin, J. A. Byars, and R. A. Brown, ''Self-similar spiral instabilities in elastic flows between a cone and a plate,'' J. Fluid Mech. **285**, 123 (1995).
[28]J. A. Byars, A. Oztekin, R. A. Brown, and G. H. McKinley, ''Spiral instabilities in the flow of highly elastic fluids between rotating parallel disks,'' J. Fluid Mech. **271**, 173 (1994).
[29]Y. Renardy and M. Renardy, ''A model equation for axisymmetric stability of small-gap parallel-plate flows,'' J. Non-Newtonian Fluid Mech. **77**, 103 (1998).
[30]R. B. Bird, C. F. Curtiss, R. C. Armstrong, and O. Hassager, *Dynamics of Polymeric Liquids: Volume 2 Kinetic Theory* (Wiley, New York, 1987).
[31]R. K. Gupta, D. A. Nguyen, and T. Sridhar, ''Extensional viscosity of dilute polystyrene solutions: Effect of concentration and molecular weight,'' Phys. Fluids **12**, 1296 (2000).
[32]J. D. Ferry, *Viscoelastic Properties of Polymers* (Wiley-Interscience, New York, 1980).
[33]S. L. Anna, G. H. McKinley, D. A. Nguyen, T. Sridhar, S. J. Muller, J. Huang, and D. F. James, ''An inter-laboratory comparison of measurements from filament stretching rheometers using common test fluids,'' J. Rheol. **45**, 83 (2001).
[34]B. H. Zimm, ''Dynamics of polymer molecules in dilute solution: viscoelasticity, flow birefringence and dielectric loss,'' J. Chem. Phys. **24**, 269 (1956).
[35]R. G. Larson, *Constitutive Equations for Polymer Melts and Solutions* (Butterworths, Boston, 1988).
[36]M. E. Mackay and D. V. Boger, ''An explanation of the rheological properties of Boger fluids,'' J. Non-Newtonian Fluid Mech. **22**, 235 (1987).
[37]H. C. Ottinger, ''Generalized Zimm model for dilute polymer-solutions under theta-conditions,'' J. Chem. Phys. **86**, 3731 (1987).
[38]R. B. Bird and J. R. DeAguiar, ''An encapsulated dumbbell model for concentrated polymer solutions and melts I. Theoretical development and constitutive equation,'' J. Non-Newtonian Fluid Mech. **13**, 149 (1983).
[39]R. G. Larson, S. J. Muller, and E. S. G. Shaqfeh, ''The effect of fluid rheology on the elastic Taylor–Couette instability,'' J. Non-Newtonian Fluid Mech. **51**, 195 (1994).
[40]U. A. Al-Mubaiyedh, R. Sureshkumar, and B. Khomami, ''Linear stability of viscoelastic Taylor–Couette flow: Influence of fluid rheology and energetics,'' J. Rheol. **44**, 1121 (2000).
[41]A. Oztekin and R. A. Brown, ''Instability of a viscoelastic fluid between rotating parallel disks: analysis for the Oldroyd-B fluid,'' J. Fluid Mech. **255**, 473 (1993).
[42]M. Arigo, ''The effects of fluid rheology on the dynamics of isothermal and nonisothermal flows of viscoelastic fluids,'' Ph.D. Thesis, Harvard University, 1999.
[43]A. Avagliano and N. Phan-Thien, ''Torsional flow stability of highly dilute polymer solutions,'' J. Non-Newtonian Fluid Mech. **84**, 19 (1999).
[44]A. Oztekin, R. A. Brown, and G. H. McKinley, ''Quantitative prediction of the viscoelastic instability in cone-and-plate flow of a Boger fluid using a multi-mode Giesekus model,'' J. Non-Newtonian Fluid Mech. **54**, 351 (1994).
[45]U. A. Al-Mubaiyedh, R. Sureshkumar, and B. Khomami, ''Energetic effects on the stability of viscoelastic Dean flow,'' J. Non-Newtonian Fluid Mech. **95**, 277 (2000).
[46]F. Heslot, B. Castaing, and A. Libchaber, ''Transition to turbulence in helium gas,'' Phys. Rev. A **36**, 5870 (1987).